mathematics

MDPI

Article

Information-Theoretic Sequential Framework to Elicit Dynamic High-Order Interactions in High-Dimensional Network Processes

Helder Pinto [1,2]*, Yuri Antonacci [3], Gorana Mijatovic [4], Laura Sparacino [3], Sebastiano Stramaglia [5], Luca Faes [3,4] and Ana Paula Rocha [1,2]

[1] Centro de Matemática da Universidade do Porto (CMUP), Departamento de Matemática, Faculdade de Ciências, Universidade do Porto, 4169-007 Porto, Portugal; aprocha@fc.up.pt
[2] Intelligent Systems Associate Laboratory (LASI), Centro Algoritmi, University of Minho, 4804-533 Guimarães, Portugal
[3] Department of Engineering, University of Palermo, 90128 Palermo, Italy; yuri.antonacci@unipa.it (Y.A.); laura.sparacino@unipa.it (L.S.); luca.faes@unipa.it (L.F.)
[4] Faculty of Technical Sciences, University of Novi Sad, 21000 Novi Sad, Serbia; gorana86@uns.ac.rs
[5] Department of Physics, University of Bari Aldo Moro, and INFN Sezione di Bari, 70126 Bari, Italy; sebastiano.stramaglia@ba.infn.it
* Correspondence: helder.pinto@fc.up.pt

Abstract

Complex networks of stochastic processes are crucial for modeling the dynamics of interacting systems, particularly those involving high-order interactions (HOIs) among three or more components. Traditional measures—such as mutual information (MI), interaction information (II), the redundancy-synergy index (RSI), and O-information (OI)—are typically limited to static analyses not accounting for temporal correlations and become computationally unfeasible in large networks due to the exponential growth of the number of interactions to be analyzed. To address these challenges, first a framework is introduced to extend these information-theoretic measures to dynamic processes. This includes the II rate (IIR), RSI rate (RSIR), and the OI rate gradient (ΔOIR), enabling the dynamic analysis of HOIs. Moreover, a stepwise strategy identifying groups of nodes (multiplets) that maximize either redundant or synergistic HOIs is devised, offering deeper insights into complex interdependencies. The framework is validated through simulations of networks composed of cascade, common drive, and common target mechanisms, modelled using vector autoregressive (VAR) processes. The feasibility of the proposed approach is demonstrated through its application in climatology, specifically by analyzing the relationships between climate variables that govern El Niño and the Southern Oscillation (ENSO) using historical climate data.

Keywords: complex systems; high order interactions; information theory; redundancy; synergy; stochastic processes; time-series analysis

MSC: 37M10; 94A17; 62H12

Academic Editors: Alejandro Ramírez-Rojas and José Rubén Luevano Enríquez

Received: 9 May 2025
Revised: 16 June 2025
Accepted: 20 June 2025
Published: 24 June 2025

Citation: Pinto, H.; Antonacci, Y.; Mijatovic, G.; Sparacino, L.; Stramaglia, S.; Faes, L.; Rocha, A.P. Information-Theoretic Sequential Framework to Elicit Dynamic High-Order Interactions in High-Dimensional Network Processes. *Mathematics* **2025**, *13*, 2081. https://doi.org/10.3390/math13132081

1. Introduction

The complexity of physical, biological, and technological systems arises from the intricate structural and functional interactions among their components. Modern science has shifted away from the reductionist view that the behavior of a networked

system—composed of multiple potentially interacting units—can be fully understood by examining each unit in isolation. Additionally, the traditional approach of modeling networked systems through pairwise measures of coupling or causality [1,2] is being increasingly questioned, as it often fails to fully capture the emergent dynamics of the system. Growing evidence indicates that network dynamics cannot be explained solely by pairwise couplings, as higher-order interactions (HOIs)—those involving multiple system components—play a crucial role in shaping the overall behavior [3,4]. As a result, new methods are being developed to incorporate these HOIs into generalized network models [5]. Higher-order relationships involving three or more systems can be redundant (where multiple interacting systems share the same information) or synergistic (where a set of systems holds some information that cannot be seen from any subset). However, implementing such approaches remains challenging, particularly when interactions need to be inferred from data, as is often the case with biological or functional networks that represent the dynamic activity of physical systems.

Information-theoretic measures have been extensively used to assess higher-order interdependences in multivariate dynamical systems across diverse fields including neuroscience [6,7], finance [8], physiology [9,10], and climatology [11], where redundancies and synergies have been found to play meaningful roles [12–16]. The partial information decomposition (PID) framework has emerged as a prominent tool for analyzing complex higher-order statistical interdependencies [12,17]. PID is able to quantify as separate quantities the synergistic and the redundant information terms together with the unique information that is held by each source but not by the others. Several approaches have been proposed relying on the PID concept and can be divided into two families: directed approaches, which decompose information provided by source systems about a target, and undirected methods disentangle shared information among stochastic processes without assigning distinct roles, capturing the interplay between redundancy and synergy while remaining invariant under permutations [18,19]. Despite the advantages of PID approaches, a key limitation is the super-exponential growth of its atoms, making full decomposition impractical for large systems. To mitigate this challenge, coarse-grained PID metrics have been introduced that bypass the computation of individual atoms by focusing on their linear combinations [20–22]. However, this approach still struggles with scalability as the number of processes in the network increases. Another approach recently introduced by Stramaglia et al. [23] proposes a method based on partial conditioning in multivariate datasets for decomposing transfer entropy (TE) [24]; the method is very versatile, as it has been extended to assess feature importance in explainable artificial intelligence [25]. Specifically, this approach bridges dyadic and polyadic methodologies, providing a complementary perspective to those focused on assessing HOIs [12,20–22]. While these methods aim to decompose the total information about the target from multiple sources, the proposed framework focuses on analyzing how the environment modifies the TE between two processes of interest.

This work builds upon [23] by introducing a stepwise strategy to identify, starting from a target node in a complex network, groups of nodes (multiplets) that maximize either redundant or synergistic HOIs. Measures traditionally applied to static analyses of random variables—such as interaction information (II) [26], the redundancy-synergy index (RSI) [27], and O-information (OI) [20]—are herein extended to the analysis of stochastic processes. Specifically, the proposed method incorporates the interaction information rate (IIR), the redundancy-synergy index rate (RSIR), and the O-information rate gradient (ΔOIR) to enable the dynamic analysis of these interactions. The approach is validated through simulations of interaction mechanisms that generate HOIs, including cascade effects, common driver, and common target motifs. Finally, its feasibility is demonstrated through the

analysis of a real-world climate network that captures the large-scale climate pattern of the El Niño–Southern Oscillation (ENSO), a key driver of global climate variability [28–30].

The article is structured as follows: Section 2 provides an overview of the proposed sequential framework, detailing its components, the mathematical formulation of the information-theoretic measures employed, and the linear parametric estimation method; Section 3 assesses the framework using two simulation scenarios, a five-variable autoregressive model and a collection of randomly generated networks with varying connection densities; finally, Section 4 illustrates the framework application to a climate network associated with ENSO variability.

The Matlab Toolbox implementing the greedy approach proposed in this work is freely available for download from the repository https://github.com/helderpinto97/GS-HOIs (accessed on 9 June 2025).

2. Sequential Method for Quantifying Higher-Order Interactions

This section outlines the methodology of the information-theoretic approach used to identify and quantify HOIs in complex networks. The section begins with a detailed presentation of the framework, introducing the IIR, RSIR, and the ΔOIR. It also includes a comprehensive discussion of the linear estimation approach used to compute these measures, highlighting its assumptions, limitations, and applicability to empirical data.

2.1. Sequential Procedure Outline

Let us consider a set consisting of M processes, $\mathbf{X} = \{X_1, \cdots, X_M\}$. This approach aims to identify, in a computationally efficient manner, a subset of processes within $\mathbf{X}$ that form an informational circuit which is the most redundant or synergistic. To achieve this, the algorithm involves the following steps:

1. Given the set $\mathbf{X}$, first identify the triplet that exhibits the highest level of redundancy or synergy according to a predefined metric.
2. Expand the selected triplet iteratively by adding one process at a time, ensuring that its inclusion results in the maximal statistically significant increase in the overall redundancy or synergy of the joint multiplet according to the chosen metric. Repeat this until no additional inclusion produces a statistically significant increase in redundancy or synergy.

The measures employed in this study to evaluate the prevalence of redundancy or synergy within a subset of processes are as follows: (i) the *interaction information rate (IIR)* [10]; (ii) the *redundancy-synergy index (RSI)* [31], extended in this work to its rate form (*RSIR*); and (iii) the *O-information rate gradient* (ΔOIR) [10]. The three measures are formulated in Equations (1), (7) and (8), respectively. The estimation details of these measures are presented in Section 2.2. Importantly, the RSIR and ΔOIR measures reduce to the IIR when applied to scenarios involving $M = 3$ processes.

Therefore, the IIR serves as the basic measure used in this work to implement Step 1 of our algorithm. The IIR for the triplet of processes $\mathbf{X_1} = \{X_{i_1}, X_{i_2}, X_{i_3}\}$, is defined as [10]:

$$I_{\mathbf{X}_1} = I_{X_{i_1};X_{i_2};X_{i_3}} = I_{X_{i_1};X_{i_2}} + I_{X_{i_1};X_{i_3}} - I_{X_{i_1};X_{i_2},X_{i_3}} \quad (1)$$

$$= I_{X_{i_1};X_{i_2}} - I_{X_{i_1};X_{i_2}|X_{i_3}}, \quad (2)$$

where $I_{(\cdot);(\cdot)}$ is the mutual information rate (MIR), which quantifies the information shared between the two processes per unit of time [32], and $I_{(\cdot);(\cdot)|(\cdot)}$ is the conditional MIR (cMIR). The IIR $I_{X_{i_1};X_{i_2};X_{i_3}} > 0$ indicates the prevalence of redundancy, while $I_{X_{i_1};X_{i_2};X_{i_3}} < 0$ indicates the prevalence of synergy. Specifically, in the former case, the knowledge of X_{i_3} reduces the information shared by X_{i_1} and X_{i_2}, indicating that the statistical dependence

between X_{i_1} and X_{i_2} is suppressed when X_{i_3} is observed. Conversely, in the latter case, the knowledge of X_{i_3} increases the information shared by X_{i_1} and X_{i_2}, indicating that the statistical dependence between X_{i_1} and X_{i_2} emerges when X_{i_3} is observed. Accordingly, step 1—identifying the most redundant or synergistic triplet—involves finding the maximum or minimum values of the IIR measure across all possible triplets within the set $\mathbf{X}$, respectively. The maximally redundant and maximally synergistic triplets identified in this way are denoted as $\mathbf{X}_1^M$ and $\mathbf{X}_1^m$, respectively.

The algorithm proceeds by iteratively selecting, for each step k ($k \geq 2$), the process $X_{i_{k+2}}^m$ such that

$$X_{i_{k+2}}^m = \underset{X_j \in \mathbf{X} \setminus \mathbf{X}_{k-1}}{\arg\min} \ \Phi_{X_j} \tag{3}$$

in the case of a search for synergy, and selecting the process $X_{i_{k+2}}^M$ such that

$$X_{i_{k+2}}^M = \underset{X_j \in \mathbf{X} \setminus \mathbf{X}_{k-1}}{\arg\max} \ \Phi_{X_j} \tag{4}$$

in the case of a search for redundancy. If the measure Φ_{X_j} is statistically significant, the process satisfying either Equations (3) or (4) is retained, updating the multiplet to $\mathbf{X}_k^m = \{\mathbf{X}_{k-1}^m, X_{i_{k+2}}^m\}$ or $\mathbf{X}_k^M = \{\mathbf{X}_{k-1}^M, X_{i_{k+2}}^M\}$, respectively, and the procedure proceeds to the next step. If Φ_{X_j} is not statistically significant, the procedure terminates, resulting in the final multiplet: $\mathbf{X}^m = \mathbf{X}_{k-1}^m$ in the case of synergy, or $\mathbf{X}^M = \mathbf{X}_{k-1}^M$ in the case of redundancy. The statistical significance of Φ_{X_j} is assessed using the surrogate-based approach [23]. Processes are added one at a time to the current multiplet to construct a set that either maximizes or minimizes Φ_{X_j}. The greedy search stops when any observed change in Φ_{X_j} can reasonably be attributed to chance. To determine this, the probability is estimated that the observed increase (or decrease) in Φ_{X_j} is smaller (or bigger) than what would result from adding a process with similar individual statistical properties but not coupled with the current multiplet $\mathbf{X}_{k-1}$.

The function $\Phi_{(\cdot)}$ applied to a process $X_j \in \mathbf{X} \setminus \mathbf{X}_1$ is the objective function of the minimization (or maximization), and is chosen in three different ways as follows. In the case (i), the conditional IIR (cIIR) is employed, where for the step $k = 2$:

$$\Phi_{X_j}^{\mathrm{IIR}} = I_{\mathbf{X}_1 | X_j}, \tag{5}$$

and for $k \geq 3$:

$$\Phi_{X_j}^{\mathrm{IIR}} = I_{\mathbf{X}_1 | X_{i_4}, \ldots, X_{i_{k+1}}, X_j}. \tag{6}$$

In the case (ii), the RSIR is employed, which, at step k is defined as [31,33]:

$$\Phi_{X_j}^{\mathrm{RSIR}} = \sum_{X_i \in \mathbf{X}_{k-1}} I_{X_j; X_i} - I_{X_j; \mathbf{X}_{k-1}}. \tag{7}$$

Finally, analogously, in case (iii), ΔOIR is used [10]:

$$\Phi_{X_j}^{\Delta\mathrm{OIR}} = \sum_{X_i \in \mathbf{X}_{k-1}} I_{X_j; \mathbf{X}_{k-1} \setminus X_i} - k I_{X_j; \mathbf{X}_{k-1}}. \tag{8}$$

In both Equations (7) and (8), $I_{(.);(.)}$ denotes the MIR.

In case (i), adding processes to the conditional vector can either increase or decrease the cIIR, revealing how the added processes interact in a synergistic or redundant way with the initial triplet $\mathbf{X}_1$. For this specific measure, the final multiplets $\mathbf{X}^M$ and $\mathbf{X}^m$ is obtained appending the initial triplet $\mathbf{X}_1$ to the conditioning vector. Regarding cases (ii) and (iii), Equations (7) and (8), the RSIR [31,33], and ΔOIR [10] quantify how the tested process X_j

contributes to the balance between redundant and synergistic interdependencies with the current multiplet $\mathbf{X}_{k-1}$.

Before delving into the technical details regarding the estimation of these information measures, it is essential to highlight that each objective function—$\Phi^{\text{IIR}}_{X_j}$, $\Phi^{\text{RSIR}}_{X_j}$, and $\Phi^{\Delta\text{OIR}}_{X_j}$—used to identify the most synergistic or redundant multiplets can be expressed as a sum of MIR terms. In particular, for $\Phi^{\text{RSIR}}_{X_j}$ and $\Phi^{\Delta\text{OIR}}_{X_j}$, this follows directly from Equations (7) and (8). Conversely, the cIIR measure can be expressed as a sum of cMIR terms. For instance, for $k = 2$, Equation (5) can be decomposed as:

$$I_{\mathbf{X_1}|X_j} = I_{X_{i_1};X_{i_2}|X_j} + I_{X_{i_1};X_{i_3}|X_j} - I_{X_{i_1};X_{i_2},X_{i_3}|X_j}. \tag{9}$$

Moreover, each cMIR term can be expressed in terms of MIR [34], leading to the following reformulation:

$$I_{\mathbf{X_1}|X_j} = I_{X_{i_1};X_{i_2},X_{i_3},X_j} - I_{X_{i_1};X_{i_2},X_j} - I_{X_{i_1};X_{i_3},X_j} + I_{X_{i_1};X_j}. \tag{10}$$

The same reasoning applies at each step k. Therefore, for each step, it suffices to estimate only MIR terms to compute the functions Φ^{IIR}, Φ^{RSIR} and $\Phi^{\Delta\text{OIR}}$. For this purpose, a parametric approach based on the vector autoregressive (VAR) model [35] is employed to estimate the MIR terms involved in the estimation of the three measures, the details of which are presented in the next section.

Another key point to emphasize is that, when analyzing real-world complex systems, the focus is often on a specific process and its interaction with the surrounding environment—particularly how other processes influence this target process, either synergistically or redundantly. This consideration can be integrated into Step 1 of the algorithm, where the selected triplet must include the predefined target process.

2.2. Linear Parametric Estimation of Higher-Order Interaction Information Measures

Consider a general system of M units, $\mathcal{S} = \{\mathcal{S}_1, \ldots, \mathcal{S}_M\}$ and focus on the two units $\mathcal{X} = \mathcal{S}_i$ and $\mathcal{Y} = \mathcal{S}_j$ while collecting the remaining $M - 2$ units in the group $\mathcal{Z} = \mathcal{S} \setminus \{\mathcal{X}, \mathcal{Y}\}$. Since the system $\mathcal{S}$ exhibits dynamic behavior, it is best described as a vector random process $S_n = [S_{1,n}, \ldots, S_{M,n}]$, where the temporal dependence is indicated by the time index n, and $S_{i,n}$ represents the sampled value of the i^{th} process at time step n ($i = 1, \ldots, M$, $n \in \mathbb{Z}$ for discrete-time processes). The equivalent notation evidencing the dynamics of the units $\{\mathcal{X}, \mathcal{Y}, \mathcal{Z}\}$ is $S_n = [X_n, Y_n, \mathbf{Z}_n]$. A widely used method to model the dynamics of $\mathbf{S} = \{X, Y, \mathbf{Z}\}$ is the linear vector autoregressive (VAR) model [35], given by:

$$\mathbf{S}_n = \sum_{k=1}^{p} \mathbf{A}_k \mathbf{S}_{n-k} + U_n \tag{11}$$

where $\mathbf{S}_n$ and $\mathbf{S}_{n-k}$ represent M-dimensional variables that capture the state of the process at the current time step n and k steps in the past, respectively. The matrix $\mathbf{A}_k$ is an $M \times M$ coefficient matrix, while U_n denotes an independent and identically distributed (i.i.d.) innovation process, with an $M \times M$ covariance matrix $\mathbf{\Sigma}_U$. Given the full model, represented in Equation (11), restricted models can be used to describe the dynamics of any given subset of processes. Specifically, the dynamics of processes X, Y, and their joint dynamics in the multivariate process $\mathbf{W} = \{X, Y\}$ are represented by:

$$\begin{aligned} X_n &= \sum_{k=1}^{q} A_k^{(x)} X_{n-k} + U_{x,n} \\ Y_n &= \sum_{k=1}^{q} A_k^{(y)} Y_{n-k} + U_{y,n} \\ \mathbf{W}_n &= \sum_{k=1}^{q} \mathbf{A}_k^{(w)} \mathbf{W}_{n-k} + \mathbf{U}_{w,n} \end{aligned} \tag{12}$$

where q is the model order (theoretically $q \to \infty$). The parameters $A_k^{(x)}$, $A_k^{(y)}$, $\mathbf{A}_k^{(w)}$, and the residual covariances Σ_{U_x}, Σ_{U_y}, $\mathbf{\Sigma}_{U_w}$, can be derived from the full model parameters $\mathbf{A}_k$ and $\mathbf{\Sigma}_U$ by solving the Yule–Walker equations and reorganizing the covariance structure of $\mathbf{S}$ to relate it to X, Y, or $\mathbf{W}$ [9].

Assuming joint Gaussianity of the overall process $\mathbf{S}$, the MIR can be directly determined from the covariances of the residuals of the restricted models:

$$I_{X;Y} = \frac{1}{2} \log \frac{\Sigma_{U_x} \cdot \Sigma_{U_y}}{|\mathbf{\Sigma}_{U_w}|}. \tag{13}$$

The aforementioned procedure can be iterated to construct restricted models that characterize the dynamics of the vector process $\mathbf{Z}$ and the joint processes $\mathbf{V} = \{X, \mathbf{Z}\}$ and $\mathbf{R} = \{Y, \mathbf{Z}\}$. These models are formulated using VAR representations, as outlined in Equation (12), enabling the derivation of expressions for the MIR terms $I_{X;\mathbf{Z}}$ and $I_{X;Y,\mathbf{Z}} = I_{X;\mathbf{R}}$:

$$I_{X;\mathbf{Z}} = \frac{1}{2} \log \frac{\Sigma_{U_x} |\mathbf{\Sigma}_{U_z}|}{|\mathbf{\Sigma}_{U_v}|}, \tag{14}$$

$$I_{X;Y,\mathbf{Z}} = I_{X;\mathbf{R}} = \frac{1}{2} \log \frac{\Sigma_{U_x} |\mathbf{\Sigma}_{U_r}|}{|\mathbf{\Sigma}_U|}. \tag{15}$$

Then, the formulations presented in Equations (13)–(15) are directly applied in Equations (10), (7), and (8) to compute Φ^{IIR}, Φ^{RSIR}, and $\Phi^{\Delta\mathrm{OIR}}$, respectively, at each step of the algorithm. In practical analyses, these metrics are computed from synchronous time series realizations of the processes X, Y, and $\mathbf{Z}$. The parameters of the full model (11) are estimated using least squares [35], and these estimates are used to derive the covariance matrices of the residuals from the restricted models [9]. These covariance matrices are then employed in Equations (13)–(15) to estimate the MIR terms. The order p of the full model is selected using the Akaike Information Criterion (AIC) [36], while the order q of the restricted models is fixed at a high value $q = 22$, in this work, to capture the decay of correlations at increasing lags [9,37]. This choice is supported by previous studies showing that, when evaluating information dynamics, all measures tend to stabilize to constant values even at relatively small lags, typically around $q = 10$ [38].

While linear approaches—such as the VAR-based method used in this study—are inherently limited to capturing linear dependencies, they offer significant advantages in analytical tractability and computational efficiency compared to model-free alternatives. Importantly, estimating information-theoretic measures using VAR models assumes a linear model, not a linear process—a subtle but crucial distinction. The linear structure of the model does not require the underlying time series to be strictly linear. Nonlinearities in the data may not compromise model stability but can result in an incomplete representation of the system dynamics [39]. Nevertheless, as long as the fitted VAR model is stable—that is, all characteristic roots (or poles) lie strictly inside the unit circle in the complex plane [35]—the resulting MIR based measures remain valid. In this setting, the model acts as a linear approximation of the system. Wold's theorem supports this view, showing

that any stationary process can be represented by a linear model, potentially of infinite order, making it potentially non-parsimonious for time series generated by a nonlinear process [40,41]. Thus, the impact of nonlinearity on the estimation is nuanced and complex. The critical question remains whether the linear model, when applied to nonlinear data, provides a sufficiently accurate representation of the underlying dynamics to make valid inferences. Though preliminary research suggests the advantages of linear models, this remains an interesting and open area for future research.

The statistical significance of the measures is assessed at each step of the algorithm. Surrogate realizations of the candidate process for the multiplet are generated using the iterative amplitude-adjusted Fourier transform (IAAFT) method, which destroys cross-correlation while preserving autocorrelation and the power spectrum [42–44]. Moreover, the IAAFT surrogates preserve the amplitude distribution of the original data, including any non-Gaussian components when present [45]. Depending on whether redundancy or synergy is being evaluated, the process is retained if the corresponding probability is above or bellow a predefined threshold, respectively. In this work, the 95% and 5% percentiles of the surrogates distribution are used as thresholds. This procedure ensures that the value obtained at each step of the algorithm is statistically significant by comparing it to surrogate data. Specifically, the same surrogate-based significance testing is applied in Step 1 to evaluate the initial triplet interaction, which is measured using the IIR. If the observed interaction passes this significance test, the algorithm proceeds; otherwise, it terminates immediately, and the selected redundancy/synergy measure are set to zero.

3. Simulation Studies

The proposed sequential method for detecting and quantifying HOIs in a network of interacting processes is validated using theoretical examples based on simulated VAR models. In these simulations, various interaction measures are computed directly from the theoretical model parameters, ensuring the evaluation of the proposed method. These simulations demonstrate how our approach can effectively identify processes that interact in a redundant or synergistic manner with respect to a predefined target process.

3.1. Five-Dimensional VAR Model

First, the proposed method is evaluated using a five-variate VAR model of order 2, defined by the following equations [7]:

$$\begin{aligned}
X_{1,n} &= 2\rho_1 \cos(2\pi f_1) X_{1,n-1} - \rho_1^2 X_{1,n-2} + (1-c) X_{2,n-1} + c X_{3,n-2} + U_{1,n}, \\
X_{2,n} &= 2\rho_2 \cos(2\pi f_2) X_{2,n-1} - \rho_2^2 X_{2,n-2} + X_{4,n-1} + U_{2,n}, \\
X_{3,n} &= 2\rho_3 \cos(2\pi f_3) X_{3,n-1} - \rho_3^2 X_{3,n-2} + X_{4,n-2} + U_{3,n}, \\
X_{4,n} &= 2\rho_4 \cos(2\pi f_4) X_{4,n-1} - \rho_4^2 X_{4,n-2} + U_{4,n}, \\
X_{5,n} &= 2\rho_5 \cos(2\pi f_5) X_{5,n-1} - \rho_5^2 X_{5,n-2} + U_{5,n},
\end{aligned} \tag{16}$$

where $\mathbf{U}_n = [U_{1,n}, \ldots, U_{5,n}]^\top$ represents a zero-mean white Gaussian noise with covariance matrix $\mathbf{\Sigma}_U$. The node X_5 represents an isolated node that does not interact with other processes in the network. The graphical representation of the model (16) is presented in Figure 1a. The parameter design in the set of Equation (16) is chosen to enable autonomous oscillations in all five processes. This is achieved by placing complex-conjugate poles in the complex plane representation of the transfer function of the vector process, with amplitudes $\rho_1, \rho_2, \rho_3, \rho_4, \rho_5$ and normalized frequency f_1, f_2, f_3, f_4, f_5. Causal interactions between processes X_2 and X_1 are controlled by the coupling parameter $1 - c$, while interactions between X_3 and X_1 are modulated by the parameter c. Specifically, the parameters were set as $\rho_1 = \rho_2 = \rho_3 = \rho_3 = \rho_5 = 0.8$, $\frac{f_1}{f_s} = \frac{f_2}{f_s} = \frac{f_3}{f_s} = \frac{f_4}{f_s} = \frac{f_5}{f_s} = 0.1$, which results in oscillatory

activity at 0.1 Hz when the sampling frequency $f_s = 1$ is considered. The parameter c was allowed to vary freely between 0 and 1.

The median and the 5th–95th percentile range of Φ_{IIR}, Φ_{RSI}, and $\Phi_{\Delta\text{OIR}}$, considering the process X_1 as target, are shown in Figure 1b, 1c, and 1d, respectively, along with the most frequently observed redundant (red) and synergistic (blue) multiplets across the 100 generated realizations. In these heatmaps, each cell is color-coded to indicate whether the process was part of the corresponding multiplet or not. The three information measures used in the $\Phi_{(.)}$ function exhibit a similar pattern: increasing c enhances synergy up to $c = 0.5$, after which it declines. Redundancy follows the opposite trend, decreasing until $c = 0.5$ and then increasing. This behavior is expected, as low c values lead to redundancy dominance due to the cascade $X_4 \to X_2 \to X_1$ [7]. At intermediate c, synergy and redundancy coexist, with synergy peaking at $c = 0.5$ due to the common child structure $X_2 \to X_1 \leftarrow X_3$, while redundancy reaches its minimum but persists due to the cascades $X_4 \to X_2 \to X_1$ and $X_4 \to X_3 \to X_1$. Beyond this point, redundancy increases while synergy declines to zero, driven by the dominance of $X_4 \to X_3 \to X_1$. This trend is captured by all three measures, though differences arise in the multiplets they identify. Φ_{IIR} clearly detects the shift between the cascades $X_4 \to X_2 \to X_1$ and $X_4 \to X_3 \to X_1$ as c increases. Meanwhile, Φ_{RSIR} and $\Phi_{\Delta\text{OIR}}$ identify $[X_1, X_2, X_3, X_4]$ as the most redundant multiplet, capturing both cascades and the common driver structure $X_2 \leftarrow X_4 \to X_3$. Regarding synergy, notable differences are observed among the Φ_{IIR}, Φ_{RSIR}, and $\Phi_{\Delta\text{OIR}}$ multiplets. In all three measures, the common empty multiplet appears at both low and high values of c, as expected, since synergy is absent in these cases and the network is dominated by cascade effects. However, at intermediate values of c, the multiplet identified by Φ_{IIR} differs from those found using Φ_{RSIR} and $\Phi_{\Delta\text{OIR}}$. The latter two measures consistently identify the multiplet $[X_1, X_2, X_3]$, revealing the common child structure $X_2 \to X_1 \leftarrow X_3$. In contrast, Φ_{IIR} also includes the process X_4 in the multiplet. Specifically, for this measure, the final multiplet is formed by extending the initial triplet with the conditioning vector (see Section 2), where X_4 is part of the conditioning vector. By incorporating X_4 into the conditioning vector, the visibility of the structure $X_2 \to X_1 \leftarrow X_3$ is enhanced. Thus, the knowledge of X_4 helps clarify the interactions between X_1, X_2, and X_3. This distinction can explain the differences observed in the multiplets identified for redundancy when using IIR when compared to RSIR and ΔOIR. In RSIR and ΔOIR, where a new process is added to the multiplet at each step, both methods detect three redundant motifs: the two cascade structures and the common driver structure $X_2 \leftarrow X_4 \to X_3$. However, since IIR is formulated in terms of conditioning, it selects processes that enhance the visibility of the interaction detected in the initial triplet rather than simply adding a new process at each step. For instance, for lower values of c, IIR identifies the dominant cascade effect $X_4 \to X_2 \to X_1$. However, no additional process is included in the conditioning vector because neither X_3 nor X_5 contains information relevant to the cascade effect detected in the first step. A similar reasoning applies to higher values of c.

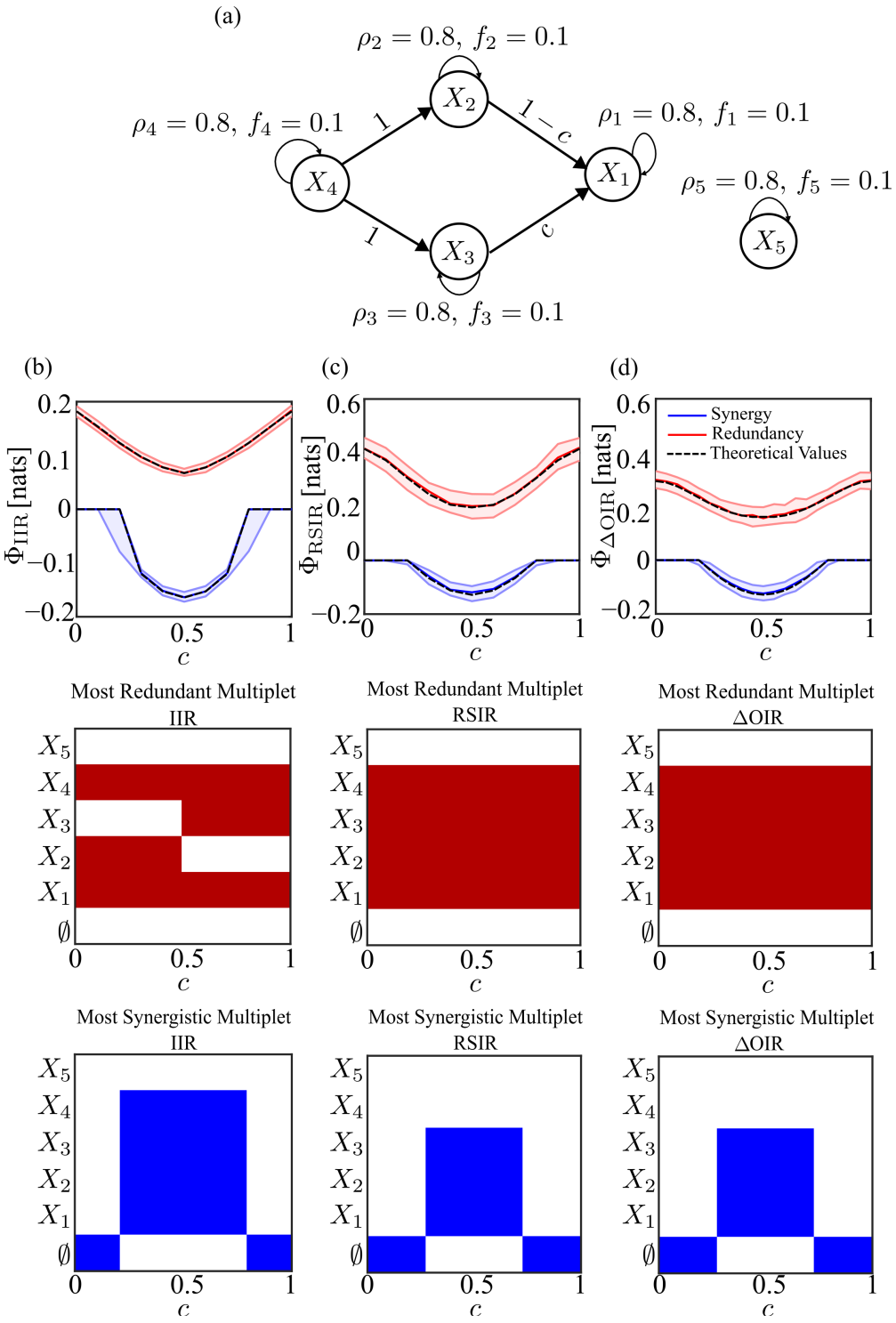

Figure 1. (**a**) Graphical representation of the five-variate VAR(2) process, generated according to Equation (16). Each node represents a distinct scalar process X_i, where $i \in \{1,2,3,4,5\}$, with arrows indicating causal interactions. Self-loops illustrate the influence of past values on the current sample. (**b**) Profiles of Φ_{IIR} for redundancy and synergy along with the theoretical value of each measure represented in black, highlighting the most redundant (red) and most synergistic (blue) multiplets. Middle and bottom plots show the most frequently observed multiplets across 100 realizations, with the colour indicating the presence of each process in the multiplet. The $\emptyset$ denotes that no multiplet was found. Similarly, panels (**c**,**d**) present the results for Φ_{RSI} and Φ_{OIR}, respectively.

3.2. Randomly Connected Networks

The simulated datasets were generated according to different ground-truth networks by means of an VAR model used as a generator filter [46]. The simulated multivariate time series ($M = 13$) were generated as realizations of a VAR process of order $p = 3$ fed by Gaussian noise with variance equal to 1. Two different matrices of AR parameters were generated by the SEED-G software according with a predefined network density of 10% and 30% (16 and 48 out of 156 possible connections). The parameters were randomly assigned in the range $[1, p]$ and their values were selected in the interval $[-0.9, 0.9]$. This value is imposed only at one lag among the possible p lags, randomly selected.

Figure 2a,b illustrate a randomly generated network with 13 nodes, featuring edge densities of 10% and 30%, respectively. The increase in density enhances connectivity, which can influence both the structural and dynamic properties of the network. Figure 2c presents the distribution of redundancy and synergy, computed using Φ_{IIR}, Φ_{RSIR}, and $\Phi_{\Delta\text{OIR}}$, based on 20 realizations of the network shown in Figure 2a. These distributions are evaluated for all possible target nodes, $X_1, \ldots, X_{13}$. Similarly, Figure 2d displays the redundancy and synergy distributions for the same three measures, obtained from 20 realizations of the denser network in Figure 2b, again considering all possible target processes, $X_1, \ldots, X_{13}$. For the network with 10% density (Figure 2c), the results show a predominance of redundancy over synergy across all information measures used in the function $\Phi_{(\cdot)}$. However, notable synergy peaks for the three measures—Φ_{IIR}, Φ_{RSIR}, and $\Phi_{\Delta\text{OIR}}$—are observed when X_2, X_8, and X_{11} are considered as target nodes. This can be explained by the common child structure $X_2 \rightarrow X_{11} \leftarrow X_8$, as seen in Figure 2a.

Increasing the network density parameter to 0.3 results in a greater number of connections, as shown in Figure 2b. Additionally, Figure 2d illustrates an increase in redundancy across all three measured parameters compared to the lower-density network, which is summarized in Figure 2c. Furthermore, as shown in Figure 2d, synergy arises when X_5, X_7, and X_{12} are considered as target processes, which can be explained by the common child structure $X_5 \rightarrow X_{12} \leftarrow X_7$. Alternatively, this can be explained by comparing the prevalence of synergistic structures involving these three nodes with that of redundant structures. All three measures considered—Φ_{IIR}, Φ_{RSIR}, and $\Phi_{\Delta\text{OIR}}$—identified the same initial triplet $[X_5, X_7, X_{12}]$. However, while RSIR and ΔOIR retained this triplet as the final multiplet, IIR included additional processes, X_2 and X_{13}, in the conditioning vector (result omitted here for simplicity). Although these two processes are associated with redundancy, as they follow the cascade $X_{13} \rightarrow X_2 \rightarrow X_{12}$, their inclusion provides valuable insight into the synergistic interactions within the initial triplet. Another important observation is that the estimated values of redundancy and synergy, calculated for the three measures across both random networks, show minimal bias when compared to the theoretical values, presented as Table 1.

Overall our simulations show that increasing network density leads to a significant rise in HOIs, as expected, because a denser network offers more connections, which helps collective behaviors to emerge. Specifically, we found that more densely connected networks exhibit a predominance of redundant interactions, which can obscure underlying synergistic effects. This behavior can be explained by the presence of common-child structures, whereas redundant interactions are more strongly linked to cascade and common-driver effects—a finding consistent with prior studies [7,10].

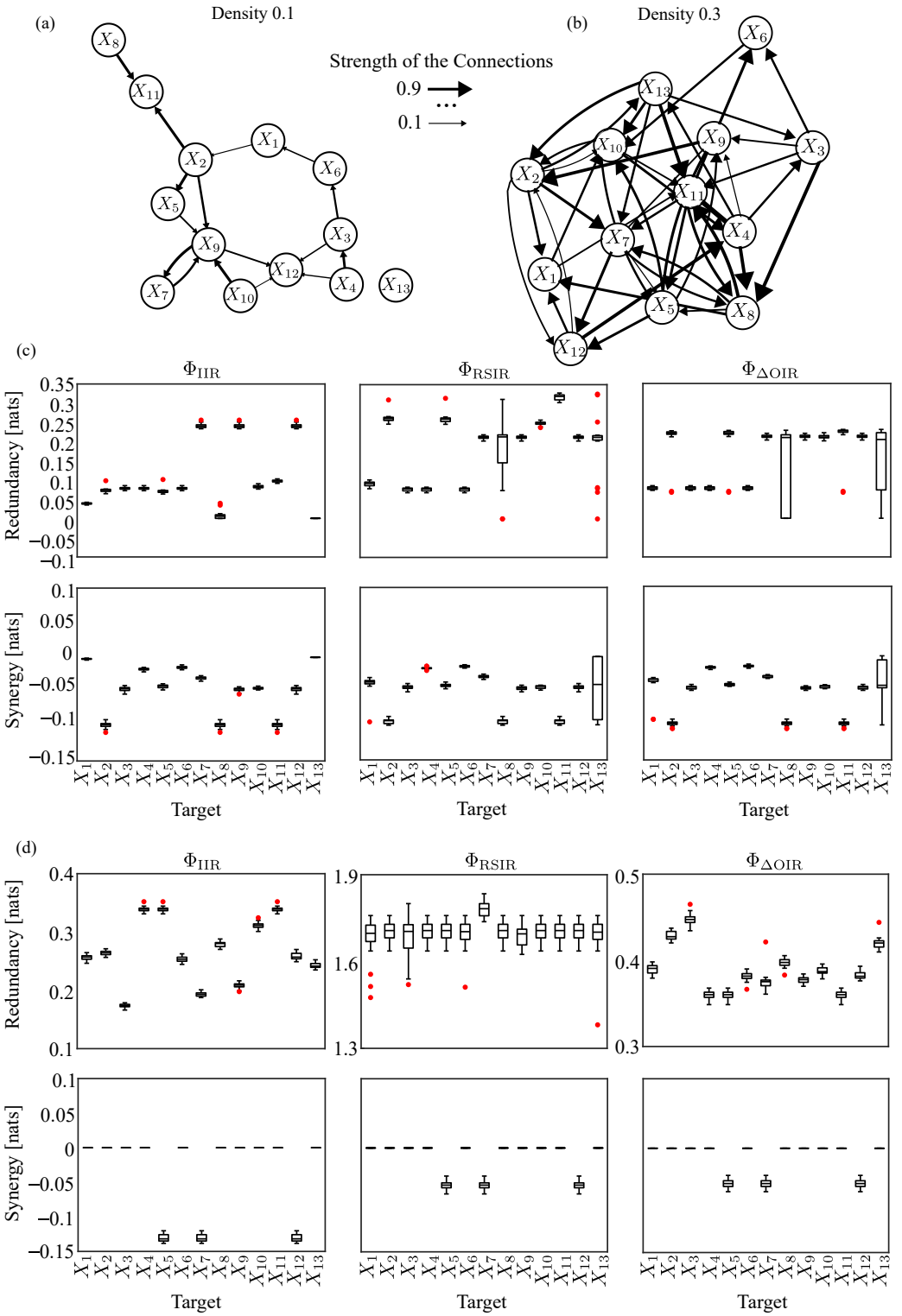

Figure 2. (**a**) Graphical representation of a random network comprising 13 nodes with a density of 0.1 and (**b**) 0.3, respectively. The width of the arrows represents the strength of interactions—the wider the arrow, the stronger the connection between processes. Panels (**c**,**d**) display the distribution of redundancy (first row) and synergy (second row) for all possible targets $X_1, \ldots, X_{13}$, computed using Φ_{IIR}, Φ_{RSIR}, and $\Phi_{\Delta\mathrm{OIR}}$ in random networks with densities of 0.1 and 0.3, respectively. Red points indicate outliers.

Table 1. Theoretical values for redundancy and synergy, for Φ_{IIR}, Φ_{RSIR}, and $\Phi_{\Delta\text{OIR}}$, obtained from the random network with parameter densities of 0.1 and 0.3, illustrated in Figure 2a and 2b, respectively.

		Measure/Target	X_1	X_2	X_3	X_4	X_5	X_6	X_7	X_8	X_9	X_{10}	X_{11}	X_{12}	X_{13}
Density 0.1	Redundancy	Φ_{IIR}	0.0391	0.0710	0.0783	0.0783	0.0690	0.0783	0.2430	0	0.2430	0.0835	0.0975	0.2430	0
		Φ_{RSIR}	0.0932	0.2589	0.0783	0.0783	0.2574	0.0783	0.2126	0.1174	0.2126	0.2482	0.3154	0.2126	0.1174
		$\Phi_{\Delta\text{OIR}}$	0.0783	0.2209	0.0783	0.0783	0.2206	0.0783	0.2126	0.1025	0.2126	0.2118	0.2252	0.2126	0.1025
	Synergy	Φ_{IIR}	−0.0026	−0.0968	−0.0457	−0.0169	−0.0419	−0.0150	−0.0296	−0.0968	−0.0457	−0.0440	−0.0968	−0.0457	0
		Φ_{RSIR}	−0.0377	−0.0968	−0.0457	−0.0169	−0.0419	−0.0150	−0.0296	−0.0968	−0.0457	−0.0440	−0.0968	−0.0457	−0.0227
		$\Phi_{\Delta\text{OIR}}$	−0.0348	−0.0968	−0.0457	−0.0169	−0.0419	−0.0150	−0.0296	−0.0968	−0.0457	−0.0440	−0.0968	−0.0457	−0.0208
Density 0.3	Redundancy	Φ_{IIR}	0.2544	0.2624	0.1728	0.3388	0.3388	0.2514	0.1921	0.2781	0.2091	0.3102	0.3388	0.2564	0.2395
		Φ_{RSIR}	1.7048	1.7048	1.6904	1.7048	1.7048	1.7048	1.7843	1.7048	1.6856	1.7048	1.7048	1.7048	1.7048
		$\Phi_{\Delta\text{OIR}}$	0.3912	0.4293	0.4472	0.3609	0.3609	0.3819	0.3739	0.3982	0.3787	0.3895	0.3609	0.3848	0.4211
	Synergy	Φ_{IIR}	0	0	0	0	−0.1368	0	−0.1368	0	0	0	0	−0.1368	0
		Φ_{RSIR}	0	0	0	0	−0.0533	0	−0.0533	0	0	0	0	−0.0533	0
		$\Phi_{\Delta\text{OIR}}$	0	0	0	0	−0.0533	0	−0.0533	0	0	0	0	−0.0533	0

4. Application to a Climate Network

The feasibility of the proposed framework is demonstrated through an exemplary case study in climate science, i.e., the network of interactions among the most representative indices descriptive of El Niño and the Southern Oscillation (ENSO) [29,30]. El Niño and the ENSO is a climate pattern involving periodic warming (El Niño) and cooling (La Niña) of the central and eastern Pacific Ocean, affecting global weather patterns through atmospheric pressure shifts [28]. ENSO is considered the most prominent form of interannual climate variability on Earth [29]. Since the exact mechanisms triggering ENSO warm and cool events are not fully understood, analyzing the statistical relationships among climate variables is crucial. The resulting network of interactions is tightly connected through various feedback loops that influence climate patterns over multiple years [30,47]. This highlights the need to study HOIs using a broader, dynamic approach.

The network considered was composed by 13 time series publicly available [30], covering the period of 66 years from 1950 to 2016: NINO34 (the East Central Tropical Pacific sea surface temperature anomaly), SOI (Southern Oscillation Index), AIR (All Indian Rainfall), AMO (Atlantic Multidecadal Oscillation), GMT (Global Mean Temperature anomaly), HURR (total number of hurricanes or named tropical storms per month in the Atlantic region), NOA (North Atlantic Oscillation of pressure anomalies over the Atlantic), NP (North Pacific pattern of sea level pressure), NTA (North Tropical Atlantic), PDO (Pacific Decadal Oscillation), QBO (Quasi-Biennial Oscillation), Sahel (Sahel Standardized Rainfall), and TSA (Tropical Southern Atlantic Index). It is important to note that these variables may not represent entirely distinct processes, as underlying latent factors could influence multiple indices simultaneously. This highlights the necessity of an analytical approach that accounts for shared information and potential interdependencies among the variables, like the one presented in this work.

As noted in Section 2.2, although the VAR model only partially captures the system's dynamics—given that climate data often exhibit nonlinear behavior—it still provides valuable insights by serving as a linear approximation. Previous studies on climate networks have demonstrated that linear models can yield meaningful representations of underlying dynamics [48], particularly in large-scale geophysical systems such as those governing ENSO [30,49,50]. Nevertheless, the results should be interpreted with appropriate caution due to the model inherent limitations. Additionally, our findings are compared with those of previous studies, especially [30], which employed a similar VAR-based approach to estimate causality measures, allowing for a direct and meaningful comparison.

Prior to the analysis, the time series were detrended and deseasonalized whenever necessary and rescaling the series to have zero mean and unitary variance [30]. The VAR model order was fixed at $p = 3$ based on AIC minimization, balancing fit and complex-

ity. The fitted model was stable, with all characteristic roots inside the unit circle [35]. Stationarity of all 13 variables was confirmed by the augmented Dickey–Fuller test at $\alpha = 0.05$, with p-values below 0.001 [51]. Residual normality assessed by the Lilliefors test [52] showed non-normality for some variables, notably HURR, Sahel and AIR with high kurtosis, while others (e.g., NP, SOI, NTA) exhibited mild, symmetric deviations due to heavy tails. Despite these departures, the residuals approximate symmetry and zero mean justify cautious use of the VAR model in subsequent analysis. Although the multivariate Portmanteau test was rejected [53] (p-value = 0.035), visual inspection revealed no severe autocorrelation or cross-correlation issues (additional figures that support this diagnostics can be found in Supplementary Material).

Figure 3 summarizes the redundant multiplets (first row in red) and synergistic multiplets (second row in blue) for all possible target processes, considering Φ_{IIR}, Φ_{RSIR}, and $\Phi_{\Delta\text{OIR}}$. First, we focus on one of the most important processes in the network: the Southern Oscillation index (SOI). A key observation is that the initial triplet identified for all three measures, regarding redundancy, was the same: $[\text{SOI}, \text{GMT}, \text{NINO34}]$. This corroborates in some extent the results presented in [30], where authors found that SOI may act as a common driver influencing both NINO34 and GMT. For Φ_{IIR}, no additional redundant processes were included in the multiplet. However, for Φ_{RSIR} and $\Phi_{\Delta\text{OIR}}$, the final multiplet expanded significantly to $[\text{SOI}, \text{GMT}, \text{NINO34}, \text{NTA}, \text{AMO}, \text{NP}, \text{PDO}]$. This expansion suggests that RSIR and ΔOIR capture a broader set of redundant motifs, potentially uncovering cascading effects such as NINO34 $\rightarrow$ AMO $\rightarrow$ SOI and NINO34 $\rightarrow$ NTA $\rightarrow$ SOI, as observed in [30]. Furthermore, this finding supports that the triplet $[\text{NINO34}, \text{PDO}, \text{SOI}]$ interacts in a redundant manner, consistent with the results reported in [54] using the partial information rate decomposition framework. Regarding synergy, for all three measures, the initial triplet that contributed to the final multiplet was the same regardless of the considered approach: $[\text{SOI}, \text{TSA}, \text{AIR}]$. This finding supports the presence of a common child structure, where SOI is influenced by the joint effects of AIR and TSA, potentially indicating an underlying atmospheric teleconnection pattern: $[\text{AIR}, \text{TSA}] \rightarrow$ SOI [30]. These results also partially align with the findings of [23], where the authors observed that the pair NTA and TSA contribute to the synergy in the pairwise interaction NINO34 $\rightarrow$ SOI. The differences observed in this study could be attributed to the methodological approaches: the measures used in the greedy framework presented here are undirected and capture HOIs in a more general sense, whereas [23] employed the conditioning of TE [24], a pairwise causality measure, to infer the presence of HOIs.

Interestingly, the HURR process was not present in any redundant or synergistic multiplet for any target considered, suggesting that this process does not play a role in the emergence of higher-order effects. This could be related with the fact is strongly influenced by ENSO, but it is generally considered an outcome rather than an active interacting variable in redundancy or synergy analyses but more as a pairwise interaction [55,56].

From Figure 3 and Table 2, it is clear that redundant interactions dominate the system behaviors over synergistic ones. This trend holds across all measures considered—Φ_{IIR}, Φ_{RSIR}, and $\Phi_{\Delta\text{OIR}}$—where synergy values remained consistently close to zero. Given the higher density of connections in the climate network [30], this result aligns with the results of the simulation studies as discussed in Section 3.2, showing that the number of pairwise connections influences the presence of HOIs, particularly redundancy.

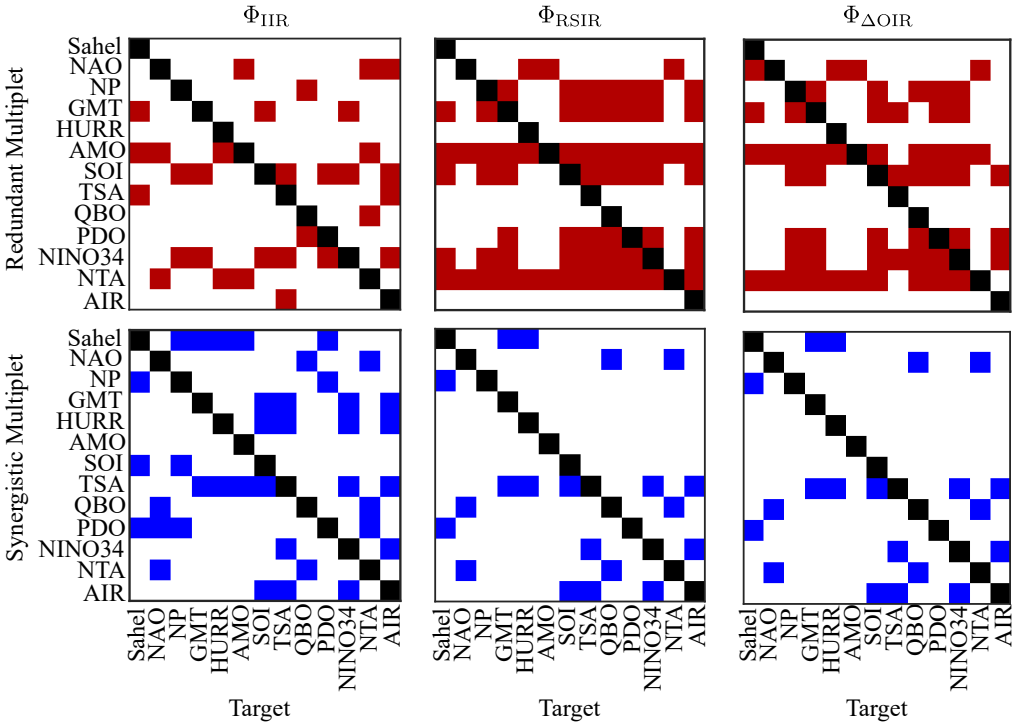

Figure 3. Heatmaps showing the most redundant (red) and most synergistic (blue) multiplets for Φ_{IIR}, Φ_{RSIR}, and $\Phi_{\Delta\mathrm{OIR}}$ across all possible targets in the considered climate network. The diagonal entries are highlighted in black to improve readability, as each target is inherently included in its corresponding multiplet. However, the focus is on identifying the processes that interact with each target.

Table 2. Values of redundancy and synergy obtained using Φ_{IIR}, Φ_{RSIR}, and $\Phi_{\Delta\mathrm{OIR}}$, considering all possible network processes as targets.

	Measure\Target	**Sahel**	**NAO**	**NP**	**GMT**	**HURR**	**AMO**	**SOI**	**TSA**	**QBO**	**PDO**	**NINO34**	**NTA**	**AIR**
Redundancy	Φ_{IIR}	0.0090	0.0194	0.0162	0.0188	0.0069	0.0194	0.0188	0.0083	0.0034	0.0185	0.0188	0.0204	0.0165
	Φ_{RSIR}	0.0514	0.0194	0.0492	0.0485	0.0213	0.0194	0.0485	0.0499	0.0591	0.0581	0.0485	0.0194	0.0636
	$\Phi_{\Delta\mathrm{OIR}}$	0.0178	0.0194	0.0237	0.0237	0.0188	0.0194	0.0237	0.0205	0.0277	0.0288	0.0237	0.0194	0.0198
Synergy	Φ_{IIR}	−0.0029	−0.0023	−0.0029	−0.0021	−0.0007	−0.0012	−0.0033	−0.0037	−0.0021	−0.0022	−0.0037	−0.0023	−0.0037
	Φ_{RSIR}	−0.0022	−0.0021	−0.0022	−0.0021	−0.0007	−0.0012	−0.0024	−0.0025	−0.0021	−0.0022	−0.0025	−0.0021	−0.0025
	$\Phi_{\Delta\mathrm{OIR}}$	−0.0022	−0.0021	−0.0022	−0.0021	−0.0007	−0.0012	−0.0024	−0.0025	−0.0021	−0.0022	−0.0025	−0.0021	−0.0025

5. Conclusions

This study introduces a novel sequential approach based on the measures IIR, RSIR, and ΔOIR to detect and quantify HOIs in complex, high-dimensional networks. The proposed method iteratively identifies multiplets that interact redundantly or synergistically with a predefined target process. By doing so, it circumvents the computational explosion associated with exhaustively considering all possible combinations, as seen in the approaches presented in [12,20,33], which scale exponentially with the number of network nodes. This makes the method particularly well-suited for analyzing large-scale systems, such as biological and climate networks, where understanding HOIs is crucial for uncovering emergent behaviors and collective dynamics.

The simulations demonstrate that the proposed method effectively detects and quantifies redundancy and synergy in complex networks. In a five-node simulation, it accurately identified both effects, aligning with theoretical expectations. In random networks, higher connection density increased high-order interactions, with redundancy becoming dominant. The application to a climate network, the method revealed strong redundancy—especially between SOI and NINO34—and identified a synergistic triplet [SOI, TSA, AIR], suggesting an atmospheric teleconnection pattern: $[\mathrm{AIR}, \mathrm{TSA}] \rightarrow \mathrm{SOI}$.

One important point to emphasize is that the linear estimation approach used to compute information-theoretic measures captures only linear interactions, which can limit its applicability to real-world networks—such as the climate networks analyzed in this work—that often exhibit nonlinear dynamics. Therefore, future work should focus on implementing this framework using model-free estimation methods, such as the nearest-neighbor approach [57], which can capture both linear and nonlinear dependencies more effectively. Despite this limitation, the proposed sequential framework demonstrates strong capability in efficiently handling complex networks with many interacting processes at relatively low computational cost. This advantage opens new avenues for exploring intricate biological systems and their interactions. In particular, the methodology shows great promise for studying physiological networks—such as cardiovascular and respiratory interactions [9,34]—as well as brain networks [58] and brain–heart interactions [59–61].

Supplementary Materials: The following supporting information can be downloaded at https://www.mdpi.com/article/10.3390/math13132081/s1, Figure S1: Residuals from the VAR(3) model for each of the 13 processes included in the fitted climate network. The red line indicates the zero reference level.; Figure S2: Histograms of the residuals from the fitted VAR(3) model for each of the 13 climate indices in the network. The overlaid orange curve represents the kernel density estimate, providing a smoothed approximation of the residual distribution for each process.; Figure S3: Sample autocorrelation functions (ACFs) of the residuals from the fitted VAR(3) model, displayed separately for each climate index, with lags up to $\tau = 10$.

Author Contributions: conceptualization, A.P.R., L.F. and G.M.; data curation, H.P.; formal analysis, H.P. and Y.A.; methodology, L.F., G.M. and A.P.R.; software, H.P.; supervision, A.P.R., L.F. and Y.A.; validation, A.P.R., L.F., G.M., Y.A. and S.S.; writing—original draft, H.P.; writing—review and editing, Y.A., G.M., L.F., L.S., S.S. and A.P.R. All authors have read and agreed to the published version of the manuscript.

Funding: The authors A.P.R and H.P were partially supported by CMUP, member of LASI, which is financed by national funds through FCT—Fundação para a Ciência e a Tecnologia, I.P., under the projects with reference UID/00144—Centro de Matemática da Universidade do Porto. H.P was supported by FCT—Fundação para a Ciência e Tecnologia, I.P. by project reference 2022.11423.BD (https://doi.org/10.54499/2022.11423.BD). Y.A. and L.F were supported by SiciliAn MicronanOTecH Research And Innovation CEnter "SAMOTHRACE" (MUR, PNRR-M4C2, ECS_00000022), spoke 3–Università degli Studi di Palermo S2-COMMs–Micro and Nanotechnologies for Smart & Sustainable Communities. G. M. was supported by the Ministry of Science, Technological Development and Innovation (Contract No. 451-03-137/2025-03/200156), and by the Faculty of Technical Sciences, University of Novi Sad, through the project "Scientific and Artistic Research Work of Researchers in Teaching and Associate Positions at the Faculty of Technical Sciences, University of Novi Sad 2025" (No. 01-50/295). S.S. was supported by the project "HONEST—High-Order Dynamical Networks in Computational Neuroscience and Physiology: an Information-Theoretic Framework", Italian Ministry of University and Research (funded by MUR, PRIN 2022, code 2022YMHNPY, CUP: B53D23003020006) and by the project "Higher-order complex systems modeling for personalized medicine", Italian Ministry of University and Research (funded by MUR, PRIN 2022-PNRR, code P2022JAYMH, CUP: H53D23009130001).

Data Availability Statement: The climate data can be downloaded at the NOAA website (https://psl.noaa.gov/data/climateindices/list/, accessed on 5 May 2025) with the exception of AIR, which is available via the Indian Institute of Tropical Meteorology (https://www.tropmet.res.in/, accessed on 5 May 2025).

Conflicts of Interest: The authors declare no conflicts of interest.

References

1. Bashan, A.; Bartsch, R.P.; Kantelhardt, J.W.; Havlin, S.; Ivanov, P.C. Network physiology reveals relations between network topology and physiological function. *Nat. Commun.* **2012**, *3*, 702. https://doi.org/10.1038/ncomms1705.
2. Bassett, D.S.; Sporns, O. Network neuroscience. *Nat. Neurosci.* **2017**, *20*, 353–364. https://doi.org/10.1038/nn.4502.
3. Battiston, F.; Cencetti, G.; Iacopini, I.; Latora, V.; Lucas, M.; Patania, A.; Young, J.G.; Petri, G. Networks beyond pairwise interactions: Structure and dynamics. *Phys. Rep.* **2020**, *874*, 1–92. https://doi.org/10.1016/j.physrep.2020.05.004.
4. Battiston, F.; Amico, E.; Barrat, A.; Bianconi, G.; de Arruda, G.F.; Franceschiello, B.; Iacopini, I.; Kéfi, S.; Latora, V.; Moreno, Y.; et al. The physics of higher-order interactions in complex systems. *Nat. Phys.* **2021**, *17*, 1093–1098. https://doi.org/10.1038/s41567-021-01371-4.
5. Bianconi, G. *Higher-Order Networks: An Introduction to Simplicial Complexes*; Cambridge University Press: Cambridge, UK, 2021; p. 140. https://doi.org/10.1017/9781108770996.
6. Antonacci, Y.; Barà, C.; Sparacino, L.; Pirovano, I.; Mastropietro, A.; Rizzo, G.; Faes, L. Spectral Information Dynamics of Cortical Signals Uncover the Hierarchical Organization of the Human Brain's Motor Network. *IEEE Trans. Biomed. Eng.* **2024**, *72*, 1655–1664. https://doi.org/10.1109/TBME.2024.3516943.
7. Antonacci, Y.; Minati, L.; Nuzzi, D.; Mijatovic, G.; Pernice, R.; Marinazzo, D.; Stramaglia, S.; Faes, L. Measuring high-order interactions in rhythmic processes through multivariate spectral information decomposition. *IEEE Access* **2021**, *9*, 149486–149505. https://doi.org/10.1109/ACCESS.2021.3124601.
8. Bardoscia, M.; Barucca, P.; Battiston, S.; Caccioli, F.; Cimini, G.; Garlaschelli, D.; Saracco, F.; Squartini, T.; Caldarelli, G. The physics of financial networks. *Nat. Rev. Phys.* **2021**, *3*, 490–507. https://doi.org/10.1038/s42254-021-00322-5.
9. Mijatovic, G.; Antonacci, Y.; Javorka, M.; Marinazzo, D.; Stramaglia, S.; Faes, L. Network Representation of Higher-Order Interactions Based on Information Dynamics. *IEEE Trans. Netw. Sci. Eng.* **2025**, *12*, 1872–1884. https://doi.org/10.1109/TNSE.2025.3540982.
10. Faes, L.; Mijatovic, G.; Antonacci, Y.; Pernice, R.; Bara, C.; Sparacino, L.; Sammartino, M.; Porta, A.; Marinazzo, D.; Stramaglia, S. A New Framework for the Time-and Frequency-Domain Assessment of High-Order Interactions in Networks of Random Processes. *IEEE Trans. Signal Process.* **2022**, *70*, 5766–5777. https://doi.org/10.1109/TSP.2022.3221892.
11. Leung, L.Y.; North, G.R. Information theory and climate prediction. *J. Clim.* **1990**, *3*, 5–14. https://doi.org/10.1175/1520-0442(1990)003<0005:ITACP>2.0.CO;2.
12. Williams, P.L.; Beer, R.D. Nonnegative Decomposition of Multivariate Information. *arXiv* **2010**, arXiv:1004.2515.
13. James, R.G.; Ellison, C.J.; Crutchfield, J.P. Anatomy of a bit: Information in a time series observation. *Chaos Interdiscip. J. Nonlinear Sci.* **2011**, *21*, 037109. https://doi.org/10.1063/1.3637494.
14. Stramaglia, S.; Cortes, J.M.; Marinazzo, D. Synergy and redundancy in the Granger causal analysis of dynamical networks. *New J. Phys.* **2014**, *16*, 105003. https://doi.org/10.1088/1367-2630/16/10/105003.
15. Barrett, A.B. Exploration of synergistic and redundant information sharing in static and dynamical Gaussian systems. *Phys. Rev. E* **2015**, *91*, 052802. https://doi.org/10.1103/PhysRevE.91.052802.
16. Finn, C.; Lizier, J.T. Pointwise partial information decomposition using the specificity and ambiguity lattices. *Entropy* **2018**, *20*, 297. https://doi.org/10.3390/e20040297.
17. Wibral, M.; Priesemann, V.; Kay, J.W.; Lizier, J.T.; Phillips, W.A. Partial information decomposition as a unified approach to the specification of neural goal functions. *Brain Cogn.* **2017**, *112*, 25–38. https://doi.org/10.1016/j.bandc.2015.09.004.
18. Rosas, F.; Ntranos, V.; Ellison, C.J.; Pollin, S.; Verhelst, M. Understanding interdependency through complex information sharing. *Entropy* **2016**, *18*, 38. https://doi.org/10.3390/e18020038.
19. Ince, R.A.A. The Partial Entropy Decomposition: Decomposing multivariate entropy and mutual information via pointwise common surprisal. *arXiv* **2017**, arXiv:1702.01591.
20. Rosas, F.E.; Mediano, P.A.; Gastpar, M.; Jensen, H.J. Quantifying high-order interdependencies via multivariate extensions of the mutual information. *Phys. Rev. E* **2019**, *100*, 032305. https://doi.org/10.1103/PhysRevE.100.032305.
21. Rosas, F.E.; Mediano, P.A.M.; Jensen, H.J.; Seth, A.K.; Barrett, A.B.; Carhart-Harris, R.L.; Bor, D. Reconciling emergences: An information-theoretic approach to identify causal emergence in multivariate data. *PLoS Comput. Biol.* **2020**, *16*, e1008289. https://doi.org/10.1371/journal.pcbi.1008289.
22. Mediano, P.A.; Rosas, F.E.; Bor, D.; Seth, A.K.; Barrett, A.B. The strength of weak integrated information theory. *Trends Cogn. Sci.* **2022**, *26*, 646–655. https://doi.org/10.1016/j.tics.2022.04.008.
23. Stramaglia, S.; Faes, L.; Cortes, J.M.; Marinazzo, D. Disentangling high-order effects in the transfer entropy. *Phys. Rev. Res.* **2024**, *6*, L032007. https://doi.org/10.1103/PhysRevResearch.6.L032007.
24. Schreiber, T. Measuring information transfer. *Phys. Rev. Lett.* **2000**, *85*, 461–464. https://doi.org/10.1103/PhysRevLett.85.461.
25. Ontivero-Ortega, M.; Faes, L.; Cortes, J.M.; Marinazzo, D.; Stramaglia, S. Assessing high-order effects in feature importance via predictability decomposition. *Phys. Rev. E* **2025**, *111*, L033301. https://doi.org/10.1103/PhysRevE.111.L033301.

26. McGill, W. Multivariate information transmission. *Trans. IRE Prof. Group Inf. Theory* **1954**, *4*, 93–111. https://doi.org/10.1109/TIT.1954.1057469.
27. Timme, N.; Alford, W.; Flecker, B.; Beggs, J.M. Synergy, redundancy, and multivariate information measures: An experimentalist's perspective. *J. Comput. Neurosci.* **2014**, *36*, 119–140. https://doi.org/10.1007/s10827-013-0458-4.
28. Timmermann, A.; An, S.I.; Kug, J.S.; Jin, F.F.; Cai, W.; Capotondi, A.; Cobb, K.; Lengaigne, M.; McPhaden, M.J.; Stuecker, M.F.; et al. El Niño–Southern Oscillation complexity. *Nature* **2018**, *559*, 535–545. https://doi.org/10.1038/s41586-018-0252-6.
29. McPhaden, M.J.; Zebiak, S.E.; Glantz, M.H. ENSO as an Integrating Concept in Earth Science. *Science* **2006**, *314*, 1740–1745. https://doi.org/10.1126/science.1132588.
30. Silini, R.; Tirabassi, G.; Barreiro, M.; Ferranti, L.; Masoller, C. Assessing causal dependencies in climatic indices. *Clim. Dyn.* **2023**, *61*, 79–89. https://doi.org/10.1007/s00382-022-06562-0.
31. Chechik, G.; Globerson, A.; Anderson, M.; Young, E.; Nelken, I.; Tishby, N. Group redundancy measures reveal redundancy reduction in the auditory pathway. In *Advances in Neural Information Processing Systems 14: Proceedings of the 2001 Conference*; MIT Press: Cambridge, MA, USA, 2001. https://doi.org/10.7551/mitpress/1120.003.0027.
32. Duncan, T.E. On the calculation of mutual information. *SIAM J. Appl. Math.* **1970**, *19*, 215–220. https://doi.org/10.1137/0119020.
33. Rosas, F.E.; Mediano, P.A.; Gastpar, M. Characterising Directed and Undirected Metrics of High-Order Interdependence. In Proceedings of the 2024 IEEE International Symposium on Information Theory Workshops (ISIT-W), Athens, Greece, 7–12 July 2024; pp. 1–6. https://doi.org/10.1109/ISIT-W61686.2024.10591754.
34. Mijatovic, G.; Sparacino, L.; Antonacci, Y.; Javorka, M.; Marinazzo, D.; Stramaglia, S.; Faes, L. Assessing High-Order Links in Cardiovascular and Respiratory Networks via Static and Dynamic Information Measures. *IEEE Open J. Eng. Med. Biol.* **2024**, *5*, 846–858. https://doi.org/10.1109/OJEMB.2024.3374956.
35. Lütkepohl, H. *New Introduction to Multiple Time Series Analysis*; Springer Science & Business Media: Berlin/Heidelberg, Germany, 2005. https://doi.org/10.1007/978-3-540-27752-1.
36. Akaike, H. A new look at the statistical model identification. *IEEE Trans. Autom. Control* **1974**, *19*, 716–723. https://doi.org/10.1109/TAC.1974.1100705.
37. Barnett, L.; Seth, A.K. The MVGC multivariate Granger causality toolbox: A new approach to Granger-causal inference. *J. Neurosci. Methods* **2014**, *223*, 50–68. https://doi.org/10.1016/j.jneumeth.2013.10.018.
38. Faes, L.; Montalto, A.; Nollo, G.; Marinazzo, D. Information decomposition of short-term cardiovascular and cardiorespiratory variability. In Proceedings of the Computing in Cardiology 2013, Zaragoza, Spain, 22–25 September 2013; pp. 113–116.
39. Barnett, L.; Seth, A.K. Granger causality for state-space models. *Phys. Rev. E-Stat. Nonlinear Soft Matter Phys.* **2015**, *91*, 040101. https://doi.org/10.1103/PhysRevE.91.040101.
40. Hannan, E.; Deistler, M. *The Statistical Theory of Linear Systems*; Classics in Applied Mathematics; Society for Industrial and Applied Mathematics: Philadelphia, PA, USA, 1988. https://doi.org/10.1137/1.9781611972191.
41. Barnett, L.; Seth, A.K. Dynamical independence: Discovering emergent macroscopic processes in complex dynamical systems. *Phys. Rev. E* **2023**, *108*, 014304. https://doi.org/10.1103/PhysRevE.108.014304.
42. Theiler, J.; Eubank, S.; Longtin, A.; Galdrikian, B.; Farmer, J.D. Testing for nonlinearity in time series: The method of surrogate data. *Phys. D Nonlinear Phenom.* **1992**, *58*, 77–94. https://doi.org/10.1016/0167-2789(92)90102-S.
43. Schreiber, T.; Schmitz, A. Improved surrogate data for nonlinearity tests. *Phys. Rev. Lett.* **1996**, *77*, 635. https://doi.org/10.1103/PhysRevLett.77.635.
44. Pinto, H.; Lazic, I.; Antonacci, Y.; Pernice, R.; Gu, D.; Barà, C.; Faes, L.; Rocha, A.P. Testing dynamic correlations and nonlinearity in bivariate time series through information measures and surrogate data analysis. *Front. Netw. Physiol.* **2024**, *4*, 1385421. https://doi.org/10.3389/FNETP.2024.1385421.
45. Lancaster, G.; Iatsenko, D.; Pidde, A.; Ticcinelli, V.; Stefanovska, A. Surrogate data for hypothesis testing of physical systems. *Phys. Rep.* **2018**, *748*, 1–60. https://doi.org/10.1016/j.physrep.2018.06.001.
46. Anzolin, A.; Toppi, J.; Petti, M.; Cincotti, F.; Astolfi, L. Seed-g: Simulated eeg data generator for testing connectivity algorithms. *Sensors* **2021**, *21*, 3632. https://doi.org/10.3390/s21113632.
47. Tsonis, A.A.; Swanson, K.L.; Roebber, P.J. What Do Networks Have to Do with Climate? *Bull. Am. Meteorol. Soc.* **2006**, *87*, 585–596. https://doi.org/10.1175/BAMS-87-5-585.
48. Runge, J. Causal network reconstruction from time series: From theoretical assumptions to practical estimation. *Chaos* **2018**, *28*, 075310. https://doi.org/10.1063/1.5025050.
49. Mosedale, T.J.; Stephenson, D.B.; Collins, M.; Mills, T.C. Granger Causality of Coupled Climate Processes: Ocean Feedback on the North Atlantic Oscillation. *J. Clim.* **2006**, *19*, 1182–1194. https://doi.org/10.1175/JCLI3653.1.
50. Runge, J.; Heitzig, J.; Marwan, N.; Kurths, J. Quantifying causal coupling strength: A lag-specific measure for multivariate time series related to transfer entropy. *Phys. Rev. E-Stat. Nonlinear Soft Matter Phys.* **2012**, *86*, 061121. https://doi.org/10.1103/PhysRevE.86.061121.

51. Dickey, D.A.; Fuller, W.A. Distribution of the Estimators for Autoregressive Time Series With a Unit Root. *J. Am. Stat. Assoc.* **1979**, *74*, 427–431. https://doi.org/10.2307/2286348.
52. Lilliefors, H.W. On the Kolmogorov-Smirnov Test for Normality with Mean and Variance Unknown. *J. Am. Stat. Assoc.* **1967**, *62*, 399–402. https://doi.org/10.1080/01621459.1967.10482916.
53. Hosking, J.R.M. The Multivariate Portmanteau Statistic. *J. Am. Stat. Assoc.* **1980**, *75*, 602–608. https://doi.org/10.1080/01621459.1980.10477520.
54. Faes, L.; Sparacino, L.; Mijatovic, G.; Antonacci, Y.; Ricci, L.; Marinazzo, D.; Stramaglia, S. Partial Information Rate Decomposition. *arXiv* **2025**, arXiv:2502.04550.
55. Smith, S.R.; Brolley, J.; O'Brien, J.J.; Tartaglione, C.A. ENSO's impact on regional U.S. hurricane activity. *J. Clim.* **2007**, *20*, 1404–1414. https://doi.org/10.1175/JCLI4063.1.
56. Rodríguez-Fonseca, B.; Suárez-Moreno, R.; Ayarzagüena, B.; López-Parages, J.; Gómara, I.; Villamayor, J.; Mohino, E.; Losada, T.; Castaño-Tierno, A. A review of ENSO influence on the North Atlantic. A non-stationary signal. *Atmosphere* **2016**, *7*, 87. https://doi.org/10.3390/atmos7070087.
57. Kraskov, A.; Stögbauer, H.; Grassberger, P. Estimating mutual information. *Phys. Rev. E* **2004**, *69*, 66138. https://doi.org/10.1103/PhysRevE.69.066138.
58. Varley, T.F.; Pope, M.; Faskowitz, J.; Sporns, O. Multivariate information theory uncovers synergistic subsystems of the human cerebral cortex. *Commun. Biol.* **2023**, *6*, 451. https://doi.org/10.1038/S42003-023-04843-W.
59. Catrambone, V.; Valenza, G. *Functional Brain-Heart Interplay: From Physiology to Advanced Methodology of Signal Processing and Modeling*; Springer International Publishing: Berlin/Heidelberg, Germany, 2021; pp. 1–236. https://doi.org/10.1007/978-3-030-79934-2.
60. Candia-Rivera, D. Brain-heart interactions in the neurobiology of consciousness. *Curr. Res. Neurobiol.* **2022**, *3*, 100050. https://doi.org/10.1016/J.CRNEUR.2022.100050.
61. Candia-Rivera, D.; Faes, L.; Fallani, F.d.V.; Chavez, M. Measures and Models of Brain-Heart Interactions. *IEEE Rev. Biomed. Eng.* 2025, *early access*. https://doi.org/10.1109/RBME.2025.3529363.